IOSR Journal of Mathematics (IOSR-JM)
e-ISSN: 2278-5728, p-ISSN: 2319-765X. Volume 19, Issue 4 Ser. 3 (July. – August. 2023), PP 01-18
www.iosrjournals.org

Pressure Distribution of a Horizontal Well in an Oil Reservoir Subject to Simultaneous Single Edged and Bottom Water Drive Mechanisms

Mutili Peter Mutisya[1*], Awuor Kennedy Otieno[1], Oyoo Daniel Okang'a[2] and Adewole Stephen Ezizanami[3]

[1]*Department of Mathematics and actuarial science, Kenyatta University, Box 43844 – 00100, Nairobi, Kenya.*
[2]*Department of Gas and Petroleum Engineering, Kenyatta University, Box 43844 – 00100, Nairobi, Kenya.*
[3]*Department of Petroleum Engineering, University of Benin, Benin City, Edo State, Nigeria.*

Abstract ***Original Research Article***

In this study the pressure distribution in an oil reservoir with a horizontal well is investigated. A horizontal well with single-edged and constant bottom pressure is outlined. A reservoir bounded with two constant pressure boundaries, like an edge and bottom water, requires that the production engineer should adhere diligently to a production schedule, developed by a reservoir engineer, for clean oil production to be possible. This means that arbitrary production practices through selection of production rates could lead to production of these external fluids. This can mar the economics of the project. Production schedules or plans show acceptable rates, well design and production time that can guarantee only clean oil production. In this study, pressure behaviour of a horizontal well drilled and completed in a reservoir subject to with simultaneous single-edged and bottom water drives is investigated in detail. All possible flow periods or patterns that can be exhibited by the well are determined. Fluid flow in oil reservoirs in real time is governed by a heterogenous diffusivity equation, which describes reservoir pressure as a function of reservoir, fluid and wellbore properties. To solve this unsteady state problem, Green's functions were deployed to represent the boundaries of the reservoir selected for study. The Green's functions selected are for flow from start of transient to late time, when all the external boundaries are felt. Newman product rule was used to derive a dimensionless pressure expression for the reservoir system oil flow. The source of pressure transient was production throughout. All the resulting integrals were performed numerically. MATLAB programming was used to plot the curves by applying spline functions interpolation. Influence of reservoir, fluid and wellbore properties on reservoir pressure was investigated in real time. To assist interpretation, dimensionless pressure derivatives were also computed. Near wellbore problems, like skin and wellbore storage, which affect well performance only at very early time, were not considered in the study. From the results, P_D and P'_D vary directly with h_D and inversely as L_D. The P'_D gradually reduces to zero when P_D begins to exhibit a constant trend. P'_D vary inversely with h_D and y_{eD} at all flow times. The number of flow periods varies with reservoir size, well length and production time. The time at which the P'_D starts to exhibit a downward trend is the external fluid breakthrough time. The breakthrough time is affected by well design. Longer wells exhibit delayed breakthrough time because of lower pressure drawdown associated with increased well length. If production rate is sustained for any particular well design, the well will completely water-out. Finally, infinite conductivity $x_D = 0.732$ and uniform flux condition do not really affect P_D and P'_D at early time.

Keywords: *Dimensionless Pressure, Bounded Oil Reservoir, Horizontal Well, Edge and Bottom Water Drive, Early Radial Flow Regime, Early Linear Flow Regime, Late Pseudo-radial Flow Regime, Late Linear Flow Regime.*

Date of Submission: 10-08-2023 Date of Acceptance: 20-08-2023

I. Introduction

Optimization of reservoir fluids in oil reservoirs is the most fundamental objective of reservoir engineers. The encroachments of unwanted reservoir fluids may mar enhanced clean oil production. Some of the problems encountered in reservoirs is edge and bottom water drive mechanisms. In view of this, the well need to be designed in such a manner to optimize the clean oil production. In this study, the effects of dimensionless pay thickness, dimensionless well length and dimensionless reservoir width on dimensionless pressure and dimensionless pressure derivative in all flow regimes of a horizontal well is analyzed in this study.

****Corresponding author, Email: petermutili@gmail.com;***

Numerous studies have been done by researchers with developments of various mathematical models analyzing pressure behavior in horizontal oil wells. Source and Green's function frequently used to solve unsteady flow problems in oil reservoirs were initially introduced by [1].

Horizontal well test design and interpretation methods was presented by [2] where analytical solutions were developed to carry out design as well as interpretation with semi log and log-log analysis which pointed out the distinctive behavior of horizontal wells. [3] discussed the performance of a horizontal well subject to bottom water drive and delineated conditions under which this completion mode is more appropriate. [4] studied pressure derivative behavior for a well located near finite – conductivity fault and expressions to estimate the distance from the well to the fault, fault conductivity and fault skin factor were introduced and successfully tested with synthetic and field examples. [5] investigated theoretically the time water will breakthrough a horizontal well placed in bottom-water reservoir and subsequently suggested ways to delay the water breakthrough time. Thus, the model herein is a repository of three aims of reservoir modeling; predict, optimize and monitor oil production. [6] discussed the effects of wellbore and reservoir properties on P_D and P_D' of a horizontal well in a reservoir. They also considered the effects of rectangular and square reservoir geometries where the results showed that P_D increases with h_D and the r_{wD} was found to be inversely related to P_D. [7] developed a technique for the interpretation of transient pressure based on dimensionless pressure and pressure derivative. They identified curve matching as one of the techniques that can be used to interpret the pressure data of horizontal wells in finite reservoirs. Their results show that the effect of the boundary on the pressure response of the horizontal wells and the type of flow regimes depend on the length of the horizontal wells and the distance to the nearest boundary**.** [8] compared dimensionless pressures and pressure derivatives computed by varying the reservoir geometry. Results presented show that the rate of decline of the pressure derivative curve is sharper and more sensitive in vertical well than horizontal well of the same geometry indicating a shorter period of clean oil production in vertical well than the horizontal well. [9] considered an isotropic reservoir throughout their study where all the flow periods, including the number of transition periods, were identified for several cases of reservoir external boundaries and horizontal well designs. The Results showed that a mandatory infinite-acting (radial flow period) initiates any flow in all cases of reservoir geometry, boundaries and well designs. Further the number of flow periods were affected by the reservoir boundaries, geometry and wellbore design showing that the number of successive flow period increases with horizontal well length as dictated by wellbore radius.

A mathematical model using Source and Green's functions for a Horizontal Wells in a Bounded Reservoir with Constant Pressure at the Top and Bottom for the interpretation of pressure responses in the reservoir based on dimensionless pressure and pressure derivative was developed by [10]. Results showed that dimensionless lateral extent does not directly affect the dimensionless pressure and dimensionless pressure derivative for very short well lengths. [11] studied the behavior of pressure in horizontal well subjected by a Gas cap at a late period using source function. The results showed that, pressure became stable when $t_D \geq 100$ indicating that reservoir fluid has encountered a boundary. He also observed that the decline rate increases with time to a point when $t_D \geq 100$. At this point, the Gas cap which acts as a drive is not active. Hence, there will be no increase in production at this stage. Therefore, well can be abandon or subject to Secondary recovery.

In this paper we are providing solutions to the mathematical models developed for early radial flow regime along a vertical plane, early linear flow regime, late pseudo-radial flow regime along horizontal plane and the late linear flow regime. This was achieved by selecting sets of fluids wellbore and reservoir properties as discussed below.

II. Reservoir Model Description

The wellbore and reservoir model are illustrated in figure 1. below. Slightly compressible fluid is considered flowing towards the horizontal well of dimensionless length, L_D. The horizontal well is considered as a line source designed such that $y_{eD} = 2y_{wD}$ with the right edge and bottom boundary permeable assuming that the skin and wellbore storage effects are negligible.

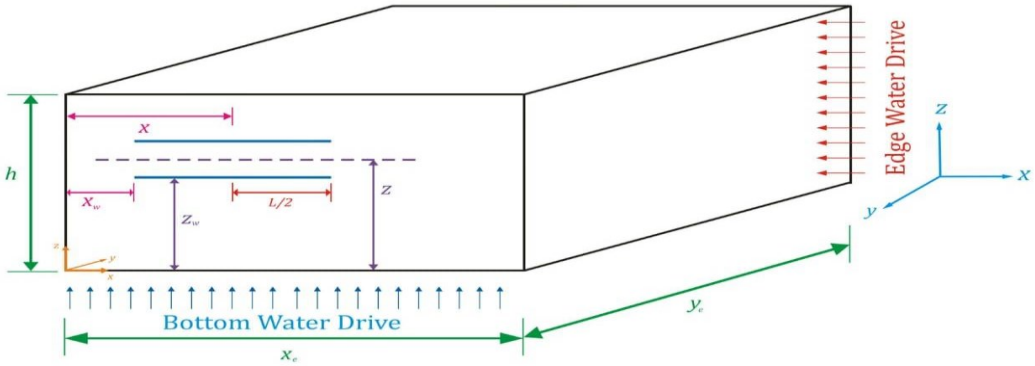

Figure 1. Oil reservoir with a horizontal well

III. Mathematical Model Description

$$P_D = \frac{kh\Delta p}{141.2q\mu B} \quad (1)$$

The quantity $\frac{q\mu}{4\pi kh}$ in Darcy units is $\frac{70.6q\mu B}{kh}$ in practical units is valid for describing the behavior of a well in a bounded reservoir during the early transient flow period prior to the occurrence of boundary effects [12].

Therefore $\frac{q\mu}{4\pi kh} = \frac{70.6q\mu B}{kh}$ (2)

Simplifying equation (2) we have: -

$$\frac{a_1}{B} = 2\pi \quad (3)$$

Where $a_1 = \frac{1}{141.2}$ in customary units.

$$P_D = \frac{a_1 kh\Delta p}{Bq\mu} \quad (4)$$

Using equation (3) in equation (4) we have: -

$$P_D = 2\pi\frac{kh\Delta P}{q\mu} \quad (5)$$

Individual horizontal segment in a horizontal slab reservoir can be considered as a line source with length, L. Using instantaneous source solutions and the Newman product principle, the pressure difference caused by the segment is given by: -

$$\Delta P = \frac{q}{\phi c_t L}\int_0^\tau s(x,t).s(y,t).s(z,t)d\tau \qquad [13] \quad (6)$$

The mathematical relationships of the axis of the fluid flow are outlined by the instantaneous point source function obtained by the Green's functions and the Newman's product rule as: -

$$P_D = \frac{2\pi kh}{\mu\phi c_t L}\int_0^\tau s(x,t).s(y,t).s(z,t)d\tau \quad (7)$$

Where $d\tau = \frac{\phi\mu c_t L^2}{4k}d\tau_D$ and $h = \frac{h_D L}{2}\sqrt{\frac{k_z}{k}}$ (8)

Early radial flow regime along vertical plane

Early radial flow period along vertical plane is governed by equation below: -

$$P_D = 2\pi h_D\int_0^{\tau_D}(Early\ x * Early\ y * Early\ z)d\tau \quad (9)$$

Dimensionless source function along $x - axis$ is given as: -

$$s(x_D,t_D) = \frac{1}{2}\left[erf\left(\frac{\frac{k}{k_x}+x_D}{2\sqrt{t_D}}\right) + erf\left(\frac{\frac{k}{k_x}-x_D}{2\sqrt{t_D}}\right)\right] \quad (10)$$

For anisotropic reservoir: -

$$\beta = \left[erf\left(\frac{\frac{k}{k_x}+x_D}{2\sqrt{t_D}}\right) + erf\left(\frac{\frac{k}{k_x}-x_D}{2\sqrt{t_D}}\right)\right] \quad (11)$$

Where: -

$$\beta = 2 \text{ when } \sqrt{\frac{k}{k_x}} > x_D \text{ ; } \beta = 1 \text{ when } \sqrt{\frac{k}{k_x}} = x_D \text{ and } \beta = 0 \text{ when } \sqrt{\frac{k}{k_x}} < x_D \quad (12)$$

In our case, $\beta = 2$ since $\sqrt{\frac{k}{k_x}} > x_D$ (13)

$$s(x_D, t_D) = \frac{\beta}{2} \quad (14)$$

Dimensionless source function along $y - axis$ is given as: -

$$s(y_D, t_D) = \frac{1}{\sqrt{\pi t_D}}\sqrt{\frac{k}{k_y}}exp\left[-\frac{(y_D - y_{wD})^2}{4t_D}\right] \quad (15)$$

Dimensionless source function along $z - axis$ is given as: -

$$s(z_D, t_D) = \frac{1}{\sqrt{\pi t_D}}\sqrt{\frac{k}{k_z}}exp\left[-\frac{(z_D - z_{wD})^2}{4t_D}\right] \quad (16)$$

For line source well $y_D = y_{wD}$ and the dimensionless wellbore radius, $r_{wD} = z_D - z_{wD}$, therefore equation (7) reduces to: -

$$P_D = \frac{1}{4L_D}\left[-Ei\left(-\frac{r_{wD}^2}{4t_{Di}}\right)\right] \quad (17)$$

For the values of the exponential integral function when the argument is less than 0.01, the following approximation can be made: -

$$-Ei(-x) = -\ln(x) - 0.577 \quad (18)$$

The dimensionless pressure derivative is obtained as: -

$$P_D' = \frac{1}{4L_D}exp\left[-\frac{r_{wD}^2}{4t_{Di}}\right] \quad (19)$$

Equation (17) and (19) gives the P_D drop and P_D' of a horizontal well when no external boundary has been felt during the infinite acting fluid flow respectively.

Early linear flow regime

The early linear flow regime is given by: -

$$P_D = 2\pi h_D \int_0^{\tau_D} (Early\ x * Early\ y * Late\ z)d\tau \quad (20)$$

The corresponding dimensionless source functions are: -

$$s(x_D, t_D) = \frac{\beta}{2} \quad (21)$$

$$s(y_D, t_D) = \frac{1}{\sqrt{\pi t_D}}\sqrt{\frac{k}{k_y}}exp\left[-\frac{(y_D - y_{wD})^2}{4t_D}\right] \quad (22)$$

$$s(z_D, t_D) = \frac{4}{h_D}\sqrt{\frac{k}{k_z}}\sum_{n=1}^{\infty} exp\left(-\frac{(2n-1)^2\pi^2 t_D}{4h_D^2}\right)\sin\frac{(2n-1)\pi z_{wD}}{2h_D}\sin\left(\frac{(2n-1)\pi z_D}{2h_D}\right) \quad (23)$$

The resulting dimensionless pressure and dimensionless pressure derivative are respectively given as: -

$$P_D = \sqrt{\frac{\pi}{t_{Di}}}\int_0^{\tau_D} exp\left[-\frac{(y_D - y_{wD})^2}{4\tau_{Di}}\right] * \sum_{n=1}^{\infty} exp\left(-\frac{(2n-1)^2\pi^2\tau_{Di}}{4h_D^2}\right)\sin\frac{(2n-1)\pi z_{wD}}{2h_D}\sin\left(\frac{(2n-1)\pi z_D}{2h_D}\right)d\tau_D \quad (24)$$

$$P_D' = \sqrt{\pi t_{Di}}\ exp\left(-\frac{(y_D - y_{wD})^2}{4\tau_{Di}}\right) * \sum_{n=1}^{\infty} exp\left(-\frac{(2n-1)^2\pi^2\tau_{Di}}{4h_D^2}\right)\sin\frac{(2n-1)\pi z_{wD}}{2h_D}\sin\left(\frac{(2n-1)\pi z_D}{2h_D}\right) \quad (25)$$

Late pseudo - radial regime along horizontal plane

The late pseudo - radial regime along horizontal plane is governed by the equation below: -

$$P_D = 2\pi h_D \int_0^{\tau_D} (Early\ x * Late\ y * Late\ z)d\tau \quad (26)$$

The corresponding dimensionless source functions are: -

$$s(x_D, t_D) = \frac{\beta}{2} \tag{27}$$

$$s(y_D, t_D) = \frac{2}{y_{eD}}\sqrt{\frac{k}{k_y}}\left(1 + 2\sum_{n=1}^{\infty} exp\left(-\frac{n^2\pi^2 t_D}{y_{eD}^2}\right) cos\left(\frac{n\pi y_{wD}}{y_{eD}}\right) cos\left(\frac{n\pi y_D}{y_{eD}}\right)\right) \tag{28}$$

$$s(z_D, t_D) = \frac{4}{h_D}\sqrt{\frac{k}{k_z}}\sum_{n=1}^{\infty} exp\left(-\frac{(2n-1)^2\pi^2 t_D}{4h_D^2}\right) \sin\frac{(2n-1)\pi z_{wD}}{2h_D} \sin\left(\frac{(2n-1)\pi z_D}{2h_D}\right) \tag{29}$$

The resulting dimensionless pressure and dimensionless pressure derivative are respectively given as: -

$$P_D = \frac{2\pi}{y_{eD}}\int_0^{\tau_D}\left(1 + 2\sum_{n=1}^{\infty} exp\left(-\frac{n^2\pi^2 t_{Di}}{y_{eD}^2}\right)\cos\left(\frac{n\pi y_{wD}}{y_{eD}}\right)\cos\left(\frac{n\pi y_D}{y_{eD}}\right)\right) * \sum_{n=1}^{\infty} exp\left(-\frac{(2n-1)^2\pi^2 t_{Di}}{4h_D^2}\right) \sin\frac{(2n-1)\pi z_{wD}}{2h_D} \sin\left(\frac{(2n-1)\pi z_D}{2h_D}\right) d\tau_D \tag{30}$$

$$P_D' = \frac{2\pi t_{Di}}{y_{eD}}\left(1 + 2\sum_{n=1}^{\infty} exp\left(-\frac{n^2\pi^2 t_{Di}}{y_{eD}^2}\right)\cos\left(\frac{n\pi y_{wD}}{y_{eD}}\right)\cos\left(\frac{n\pi y_D}{y_{eD}}\right)\right) * \sum_{n=1}^{\infty} exp\left(-\frac{(2n-1)^2\pi^2 t_{Di}}{4h_D^2}\right) \sin\frac{(2n-1)\pi z_{wD}}{2h_D} \sin\left(\frac{(2n-1)\pi z_D}{2h_D}\right) \tag{31}$$

Late linear flow regime

The late time linear flow period is governed by the equation below: -

$$P_D = 2\pi h_D \int_0^{\tau_D} (Late\ x * Late\ y * Late\ z) d\tau \tag{32}$$

The corresponding dimensionless source functions are: -

$$s(x_D, t_D) = \frac{8}{\pi}\sum_{n=1}^{\infty}\frac{1}{n+1} exp\left(-\frac{(2n+1)^2\pi^2 t_D}{4x_{eD}^2}\right) \sin\left(\frac{(2n+1)\pi x_{wD}}{2x_{eD}}\right) \cos\left(\frac{(2n+1)\pi x_D}{2x_{eD}}\right) \cos\left(\frac{(2n+1)\pi x_D}{2x_{eD}}\right) \tag{33}$$

$$s(y_D, t_D) = \frac{2}{y_{eD}}\sqrt{\frac{k}{k_y}}\left(1 + 2\sum_{n=1}^{\infty} exp\left(-\frac{n^2\pi^2 t_D}{y_{eD}^2}\right)\cos\left(\frac{n\pi y_{wD}}{y_{eD}}\right)\cos\left(\frac{n\pi y_D}{y_{eD}}\right)\right) \tag{34}$$

$$s(z_D, t_D) = \frac{4}{h_D}\sqrt{\frac{k}{k_z}}\sum_{n=1}^{\infty} exp\left(-\frac{(2n-1)^2\pi^2 t_D}{4h_D^2}\right) \sin\frac{(2n-1)\pi z_{wD}}{2h_D} \sin\left(\frac{(2n-1)\pi z_D}{2h_D}\right) \tag{35}$$

The resulting dimensionless pressure and dimensionless pressure derivative [14] are respectively given as: -

$$P_D = \frac{16}{y_{eD}}\int_0^{\tau_D}\left[\sum_{n=1}^{\infty}\frac{1}{n+1} exp\left(-\frac{(2n+1)^2\pi^2\tau_{Di}}{4x_{eD}^2}\right) \sin\left(\frac{(2n+1)\pi x_{wD}}{2x_{eD}}\right) \cos\left(\frac{(2n+1)\pi x_D}{2x_{eD}}\right) \cos\left(\frac{(2n+1)\pi x_D}{2x_{eD}}\right) * \left(1 + 2\sum_{n=1}^{\infty} exp\left(-\frac{n^2\pi^2\tau_{Di}}{y_{eD}^2}\right)\cos\left(\frac{n\pi y_{wD}}{y_{eD}}\right)\cos\left(\frac{n\pi y_D}{y_{eD}}\right)\right) * \sum_{n=1}^{\infty} exp\left(-\frac{(2n-1)^2\pi^2\tau_{Di}}{4h_D^2}\right) \sin\left(\frac{(2n-1)\pi z_{wD}}{2h_D}\right) \sin\left(\frac{(2n-1)\pi z_D}{2h_D}\right)\right] d\tau_D \tag{36}$$

$$P_D' = \frac{16t_{Di}}{y_{eD}} * \left[\sum_{n=1}^{\infty}\frac{1}{n+1}exp\left(-\frac{(2n+1)^2\pi^2\tau_{Di}}{4x_{eD}^2}\right)\sin\left(\frac{(2n+1)\pi x_{wD}}{2x_{eD}}\right)\cos\left(\frac{(2n+1)\pi x_D}{2x_{eD}}\right)\cos\left(\frac{(2n+1)\pi x_D}{2x_{eD}}\right) * \left(1+2\sum_{n=1}^{\infty}exp\left(-\frac{n^2\pi^2\tau_{Di}}{y_{eD}^2}\right)\cos\left(\frac{n\pi y_{wD}}{y_{eD}}\right)\cos\left(\frac{n\pi y_D}{y_{eD}}\right)\right) * \sum_{n=1}^{\infty}exp\left(-\frac{(2n-1)^2\pi^2\tau_{Di}}{4h_D^2}\right)\sin\left(\frac{(2n-1)\pi z_{wD}}{2h_D}\right)\sin\left(\frac{(2n-1)\pi z_D}{2h_D}\right)\right] \quad (37)$$

The final P_D equation for all flow regimes is given by: -

$$P_D = -\frac{1}{4L_D}Ei\left(-\frac{r_{wD}^2}{4t_{Di}}\right) + \sqrt{\frac{\pi}{t_{Di}}}\int_0^{\tau_D} exp\left[-\frac{(y_D-y_{wD})^2}{4\tau_{Di}}\right] * \sum_{n=1}^{\infty}exp\left(-\frac{(2n-1)^2\pi^2\tau_{Di}}{4h_D^2}\right)\sin\frac{(2n-1)\pi z_{wD}}{2h_D}\sin\left(\frac{(2n-1)\pi z_D}{2h_D}\right)d\tau_D + \frac{2\pi}{y_{eD}}\int_0^{\tau_D}\left(1+2\sum_{n=1}^{\infty}exp\left(-\frac{n^2\pi^2t_{Di}}{y_{eD}^2}\right)\cos\left(\frac{n\pi y_{wD}}{y_{eD}}\right)\cos\left(\frac{n\pi y_D}{y_{eD}}\right)\right) * \sum_{n=1}^{\infty}exp\left(-\frac{(2n-1)^2\pi^2t_{Di}}{4h_D^2}\right)\sin\frac{(2n-1)\pi z_{wD}}{2h_D}\sin\left(\frac{(2n-1)\pi z_D}{2h_D}\right)d\tau_D + \frac{16}{y_{eD}}\int_0^{\tau_D}\left[\sum_{n=1}^{\infty}\frac{1}{n+1}exp\left(-\frac{(2n+1)^2\pi^2\tau_{Di}}{4x_{eD}^2}\right)\sin\left(\frac{(2n+1)\pi x_{wD}}{2x_{eD}}\right)\cos\left(\frac{(2n+1)\pi x_D}{2x_{eD}}\right)\cos\left(\frac{(2n+1)\pi x_D}{2x_{eD}}\right) * \left(1+2\sum_{n=1}^{\infty}exp\left(-\frac{n^2\pi^2\tau_{Di}}{y_{eD}^2}\right)\cos\left(\frac{n\pi y_{wD}}{y_{eD}}\right)\cos\left(\frac{n\pi y_D}{y_{eD}}\right)\right) * \sum_{n=1}^{\infty}exp\left(-\frac{(2n-1)^2\pi^2\tau_{Di}}{4h_D^2}\right)\sin\left(\frac{(2n-1)\pi z_{wD}}{2h_D}\right)\sin\left(\frac{(2n-1)\pi z_D}{2h_D}\right)\right]d\tau_D \quad (38)$$

The final P_D' equation for all flow regimes is given by: -

$$P_D' = \frac{1}{4L_D}exp\left[-\frac{r_{wD}^2}{4t_{Di}}\right] + \sqrt{\pi t_{Di}}\,exp\left(-\frac{(y_D-y_{wD})^2}{4\tau_{Di}}\right) * \sum_{n=1}^{\infty}exp\left(-\frac{(2n-1)^2\pi^2\tau_{Di}}{4h_D^2}\right)\sin\frac{(2n-1)\pi z_{wD}}{2h_D}\sin\left(\frac{(2n-1)\pi z_D}{2h_D}\right) + \frac{2\pi t_{Di}}{y_{eD}}\left(1+2\sum_{n=1}^{\infty}exp\left(-\frac{n^2\pi^2t_{Di}}{y_{eD}^2}\right)\cos\left(\frac{n\pi y_{wD}}{y_{eD}}\right)\cos\left(\frac{n\pi y_D}{y_{eD}}\right)\right) * \sum_{n=1}^{\infty}exp\left(-\frac{(2n-1)^2\pi^2t_{Di}}{4h_D^2}\right)\sin\frac{(2n-1)\pi z_{wD}}{2h_D}\sin\left(\frac{(2n-1)\pi z_D}{2h_D}\right) + \frac{16t_{Di}}{y_{eD}}\left[\sum_{n=1}^{\infty}\frac{1}{n+1}exp\left(-\frac{(2n+1)^2\pi^2t_{Di}}{4x_{eD}^2}\right)\sin\left(\frac{(2n+1)\pi x_{wD}}{2x_{eD}}\right)\cos\left(\frac{(2n+1)\pi x_D}{2x_{eD}}\right)\cos\left(\frac{(2n+1)\pi x_D}{2x_{eD}}\right) * \left(1+2\sum_{n=1}^{\infty}exp\left(-\frac{n^2\pi^2t_{Di}}{y_{eD}^2}\right)\cos\left(\frac{n\pi y_{wD}}{y_{eD}}\right)\cos\left(\frac{n\pi y_D}{y_{eD}}\right)\right) * \sum_{n=1}^{\infty}exp\left(-\frac{(2n-1)^2\pi^2t_{Di}}{4h_D^2}\right)\sin\left(\frac{(2n-1)\pi z_{wD}}{2h_D}\right)\sin\left(\frac{(2n-1)\pi z_D}{2h_D}\right)\right] \quad (39)$$

IV. Methodology and demonstration of the Problem

In this study, for the interpretation of the results we have used the cubic spline data interpolation. Splines are popular curves which are simple to construct and are characterized by accuracy of evaluation, ease and capacity to approximate complex shapes, interactive curve design and curve fitting. Consider the following numerical data of rock, fluid and reservoir characteristics in an infinite acting reservoir: -

$L = 500ft, 1000ft, 1500ft, 2000ft, 2500ft, 3000ft, 3500ft, x = x_w = 134ft,$
$y = y_w = 200ft, z = 160.5ft, z_w = 160ft, x_e = 6000ft, y_e = 400ft, z_e = 200ft,$
$h = 200ft, d_x = 134ft, d_y = 200ft, d_z = 160ft, D_x = 634ft, D_y = 201ft, D_z = 161ft, k_x = 22md, k_y = 16md, k_z = 20md,$ $\sqrt{\frac{k}{k_x}} = 0.9335,$ $\sqrt{\frac{k}{k_y}} = 1.0946,$ $\sqrt{\frac{k}{k_z}} = 0.9790,$
$\sqrt{\frac{k_h}{k_v}} = 0.9685.$ Hence $k = \sqrt[3]{k_x.k_y.k_z} = 19.17md$, For a horizontal well; $k_v > k_h$ where
$k_v = k_z$ and $k_h = \sqrt{k_x k_y} = 18.76md$

The following tables and figures were used to analyse the relationship between dimensionless variables and the dimensionless pressure and derivatives of a horizontal well in a rectangular reservoir geometry. Computation of dimensionless parameters, dimensionless pressure and dimensionless pressure derivatives are analysed in tables and figures below.

Table I: Calculated dimensionless fluid, reservoir and wellbore data, $x_D = 0.5000$

Dimensionless parameter	$L(ft)$	500	1000	1500	2000	2500	3000	3500
	L_D	1.1669	2.3338	3.5006	4.6675	5.8344	7.0013	8.1681
	h_D	0.7832	0.3916	0.2611	0.1958	0.1566	0.1305	0.1119
x_D		0.5000	0.5000	0.5000	0.5000	0.5000	0.5000	0.5000
y_D		0.8757	0.4378	0.2919	0.2189	0.1751	0.1459	0.1251
z_D		0.6285	0.2653	0.1442	0.0837	0.0474	0.0232	0.0059
x_{wD}		0.5000	0.5000	0.5000	0.5000	0.5000	0.5000	0.5000
y_{wD}		0.8757	0.4378	0.2919	0.2189	0.1751	0.1459	0.1251
z_{wD}		0.6266	0.2643	0.1436	0.0832	0.0470	0.0228	0.0056
x_{eD}		22.404	11.155	7.4058	5.5310	4.4061	3.6562	3.1206
y_{eD}		1.7514	0.8757	0.5838	0.4378	0.3503	0.2919	0.2502
z_{eD}		0.7832	0.3427	0.1958	0.1224	0.0783	0.0490	0.0280
r_{wD}		0.0019	0.0010	0.0006	0.0005	0.0004	0.0004	0.0003
$\propto$		1.4783	4.9891	8.5536	10.146	8.6521	4.6448	0.8547
$\propto_1$		3.6430	12.274	20.991	24.785	20.917	10.823	1.2801

Where: -

$$\propto = \frac{9}{x_{eD}^2}\sin\left(\frac{3\pi x_{wD}}{2x_{eD}}\right)\cos\left(\frac{3\pi x_D}{2x_{eD}}\right)\cos\left(\frac{3\pi x_D}{2x_{eD}}\right) + \frac{1}{h_D^2}\sin\left(\frac{\pi z_{wD}}{2h_D}\right)\sin\left(\frac{\pi z_D}{2h_D}\right) \quad (40)$$

$$\propto_1 = \frac{\pi^2}{4h_D^2}\sin\left(\frac{\pi z_{wD}}{2h_D}\right)\sin\left(\frac{\pi z_D}{2h_D}\right) \quad (41)$$

Table II: P_D and P'_D with varying t_D for all flow regimes, $L_D = 1.1669$

	$L_D = 1.1669, y_{eD} = 1.7514, h_D = 0.7832$					
	x_D	0.0000	0.5000		0.7320	
	$\propto$	1.4765	1.4783		1.4792	
	$\propto_1$	3.6430	3.6430		3.6430	
t_D	P_D	P'_D	P_D	P'_D	P_D	P'_D
0.00	0.0000	0.0000	0.0000	0.0000	0.0000	0.0000
0.05	3.6965	1.5641	3.6964	1.5639	3.6964	1.5639
0.10	4.8851	2.3032	4.8848	2.3028	4.8847	2.3026
0.15	5.8080	2.7365	5.8075	2.7357	5.8073	2.7353
0.20	6.5513	2.9581	6.5505	2.9569	6.5501	2.9563

0.25	7.1574	3.0308	7.1564	3.0293	7.1559	3.0285
0.30	7.6551	3.0002	7.6537	2.9984	7.6530	2.9975
0.35	8.0651	2.8998	8.0634	2.8977	8.0626	2.8967
0.40	8.4035	2.7544	8.4015	2.7521	8.4005	2.7510
0.45	8.6834	2.5820	8.6812	2.5796	8.6801	2.5784
0.50	8.9151	2.3960	8.9126	2.3936	8.9114	2.3923
0.55	9.1081	2.2058	9.1053	2.2033	9.1040	2.2021
0.60	9.2679	2.0182	9.2650	2.0157	9.2635	2.0145
0.65	9.3993	1.8377	9.3962	1.8353	9.3946	1.8341
0.70	9.5093	1.6670	9.5060	1.6647	9.5043	1.6636
0.75	9.6012	1.5081	9.5977	1.5059	9.5960	1.5048
0.80	9.6761	1.3617	9.6725	1.3596	9.6707	1.3586

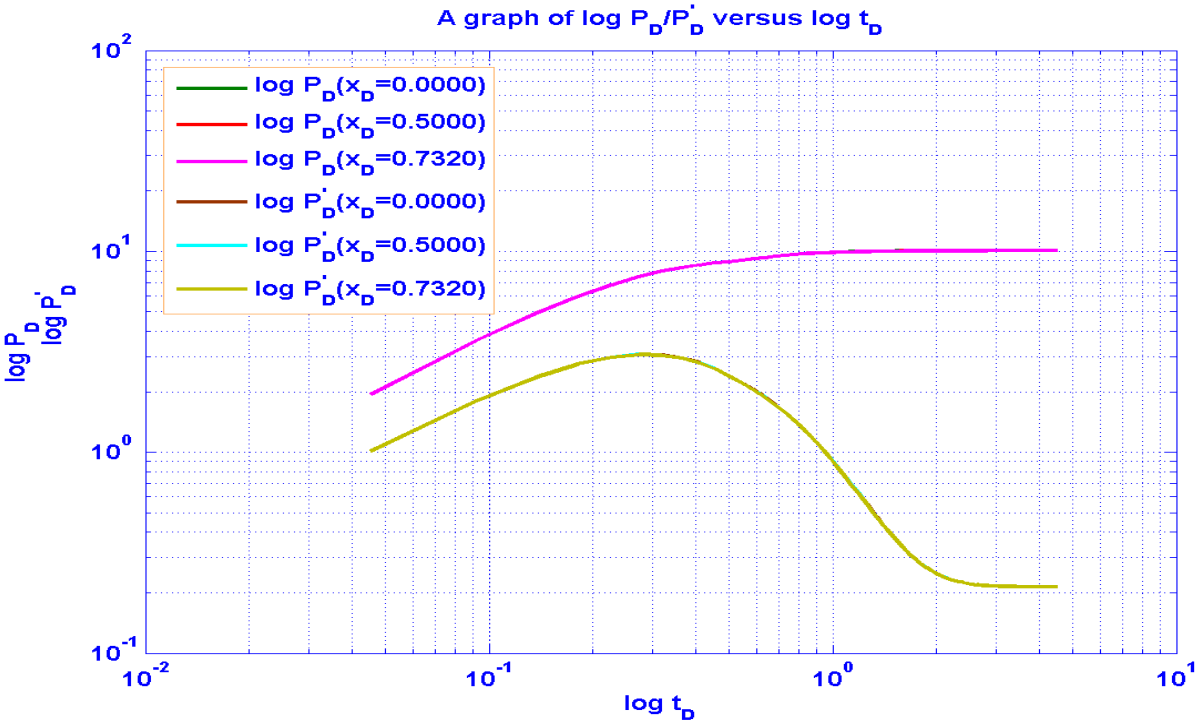

Figure 2: Graph of $\log P_D$ and $\log P'_D$ for all flow regimes, $L_D = 1.1669$

Table III: P_D and P'_D with varying t_D for all flow regimes, $L_D = 2.3338$

	$L_D = 2.3338, y_{eD} = 0.8757, h_D = 0.3916$					
	x_D	0.0000	0.5000		0.7320	
	$\propto$	4.9746	4.9891		4.9945	
	$\propto_1$	12.274	12.274		12.274	
t_D	P_D	P'_D	P_D	P'_D	P_D	P'_D
0.00	0.0000	0.0000	0.0000	0.0000	0.0000	0.0000
0.05	3.3704	1.6461	3.3696	1.6448	3.3693	1.6443
0.10	4.4611	1.7053	4.4589	1.7025	4.4580	1.7014
0.15	5.0310	1.3803	5.0275	1.3769	5.0261	1.3756
0.20	5.3336	1.0156	5.3290	1.0123	5.3273	1.0110
0.25	5.4947	0.7170	5.4895	0.7142	5.4875	0.7131
0.30	5.5810	0.5009	5.5752	0.4987	5.5731	0.4979
0.35	5.6272	0.3547	5.6212	0.3530	5.6190	0.3524
0.40	5.6523	0.2597	5.6461	0.2586	5.6438	0.2582
0.45	5.6660	0.1998	5.6597	0.1990	5.6574	0.1988
0.50	5.6741	0.1627	5.6677	0.1622	5.6654	0.1620
0.55	5.6789	0.1401	5.6725	0.1398	5.6701	0.1397
0.60	5.6821	0.1266	5.6757	0.1264	5.6733	0.1263
0.65	5.6847	0.1185	5.6782	0.1184	5.6758	0.1183
0.70	5.6869	0.1137	5.6804	0.1136	5.6780	0.1136
0.75	5.6887	0.1109	5.6822	0.1109	5.6798	0.1109
0.80	5.6903	0.1093	5.6838	0.1093	5.6814	0.1093

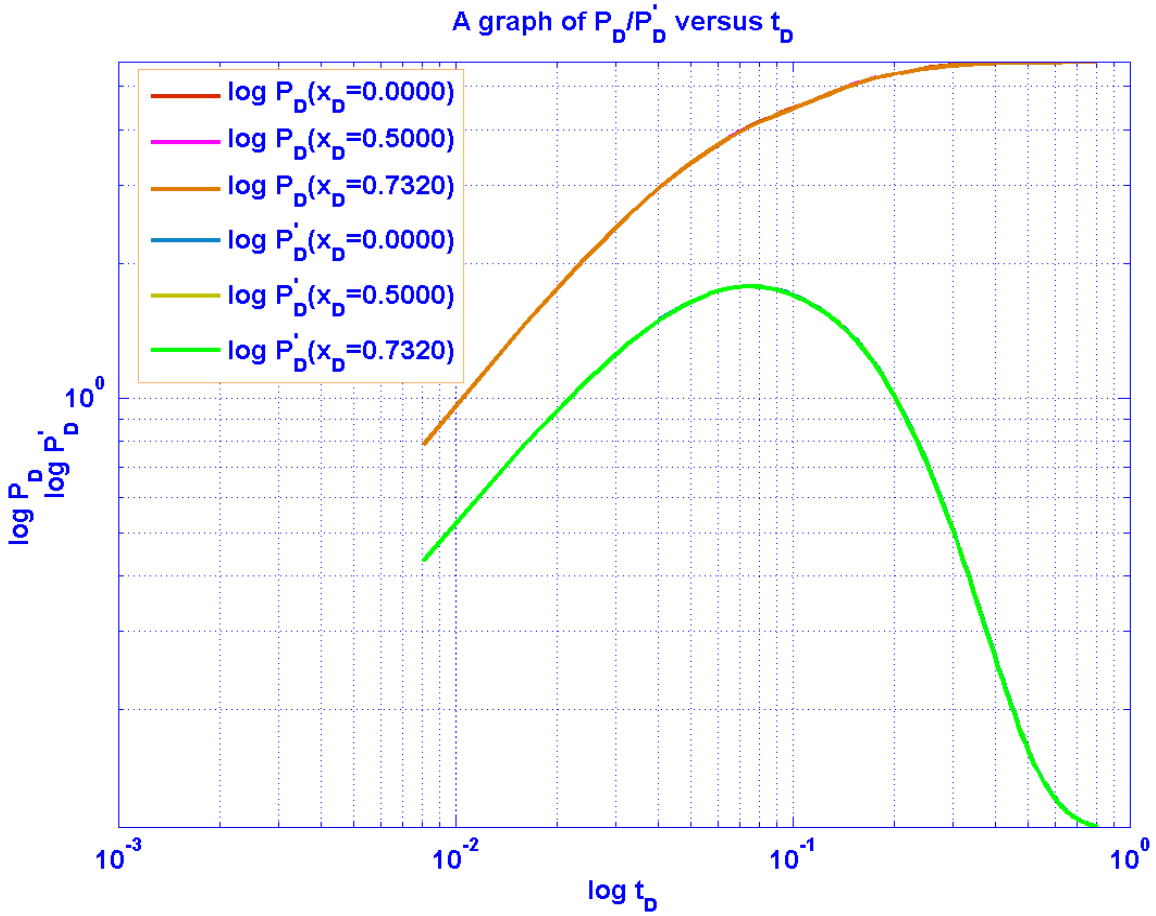

Figure 3: Graph of $\log P_D$ and $\log P'_D$ for all flow regimes, $L_D = 2.3338$

Table IV: P_D and P'_D with varying t_D for all flow regimes, $L_D = 3.5006$

	$L_D = 3.5006$, $y_{eD} = 0.5838$, $h_D = 0.2611$					
	x_D	0.0000	0.5000		0.7320	
	$\propto$	8.5072	8.5536		8.5661	
	$\propto_1$	20.991	20.991		20.991	
t_D	P_D	P'_D	P_D	P'_D	P_D	P'_D
0.00	0.0000	0.0000	0.0000	0.0000	0.0000	0.0000
0.05	3.4214	1.4950	3.4184	1.4909	3.4176	1.4898
0.10	4.2553	1.0397	4.2487	1.0340	4.2470	1.0324
0.15	4.5372	0.5733	4.5285	0.5688	4.5262	0.5676
0.20	4.6327	0.3038	4.6229	0.3010	4.6202	0.3003
0.25	4.6647	0.1727	4.6544	0.1711	4.6517	0.1707
0.30	4.6755	0.1137	4.6650	0.1129	4.6622	0.1127
0.35	4.6795	0.0886	4.6690	0.0883	4.6661	0.0882
0.40	4.6813	0.0783	4.6707	0.0781	4.6679	0.0781
0.45	4.6826	0.0741	4.6720	0.0740	4.6692	0.0740
0.50	4.6838	0.0725	4.6732	0.0724	4.6704	0.0724
0.55	4.6852	0.0718	4.6745	0.0718	4.6717	0.0718
0.60	4.6866	0.0716	4.6760	0.0715	4.6731	0.0715
0.65	4.6883	0.0715	4.6777	0.0715	4.6748	0.0715
0.70	4.6893	0.0714	4.6787	0.0714	4.6758	0.0714
0.75	4.6911	0.0714	4.6805	0.0714	4.6776	0.0714
0.80	4.6923	0.0714	4.6817	0.0714	4.6788	0.0714

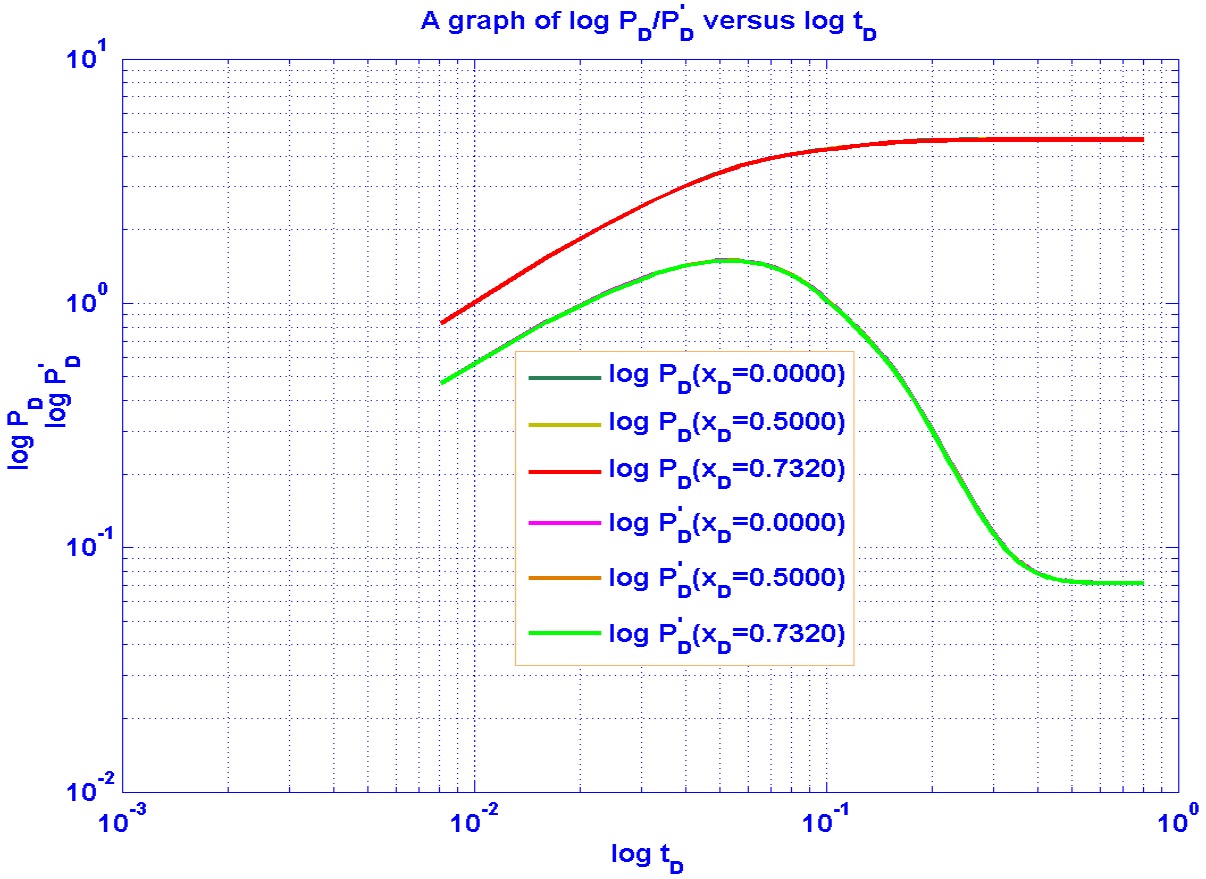

Figure 4: Graph of $\log P_D$ and $\log P'_D$ for all flow regimes, $L_D = 3.5006$

Table V: P_D and P'_D with varying t_D for all flow regimes, $L_D = 4.6675$

	$L_D = 4.6675, y_{eD} = 0.4378, h_D = 0.1958$					
	x_D	0.0000	0.5000		0.7320	
	$\propto$	10.045	10.146		10.158	
	$\propto_1$	24.785	24.785		24.785	
t_D	P_D	P'_D	P_D	P'_D	P_D	P'_D
0.00	0.0000	0.0000	0.0000	0.0000	0.0000	0.0000
0.05	3.7297	1.5856	3.7219	1.5758	3.7210	1.5746
0.10	4.5593	0.9215	4.5436	0.9101	4.5418	0.9088
0.15	4.7892	0.4269	4.7696	0.4196	4.7673	0.4187
0.20	4.8512	0.1969	4.8301	0.1932	4.8276	0.1927
0.25	4.8669	0.1052	4.8452	0.1035	4.8426	0.1033
0.30	4.8703	0.0715	4.8484	0.0708	4.8458	0.0707
0.35	4.8703	0.0596	4.8483	0.0593	4.8458	0.0593
0.40	4.8704	0.0556	4.8485	0.0555	4.8459	0.0555
0.45	4.8703	0.0542	4.8483	0.0542	4.8457	0.0542
0.50	4.8705	0.0538	4.8485	0.0538	4.8459	0.0538
0.55	4.8707	0.0537	4.8487	0.0537	4.8461	0.0537
0.60	4.8715	0.0536	4.8495	0.0536	4.8469	0.0536
0.65	4.8721	0.0536	4.8501	0.0536	4.8475	0.0536
0.70	4.8729	0.0536	4.8509	0.0536	4.8483	0.0536
0.75	4.8737	0.0536	4.8517	0.0536	4.8491	0.0536
0.80	4.8745	0.0536	4.8525	0.0536	4.8499	0.0536

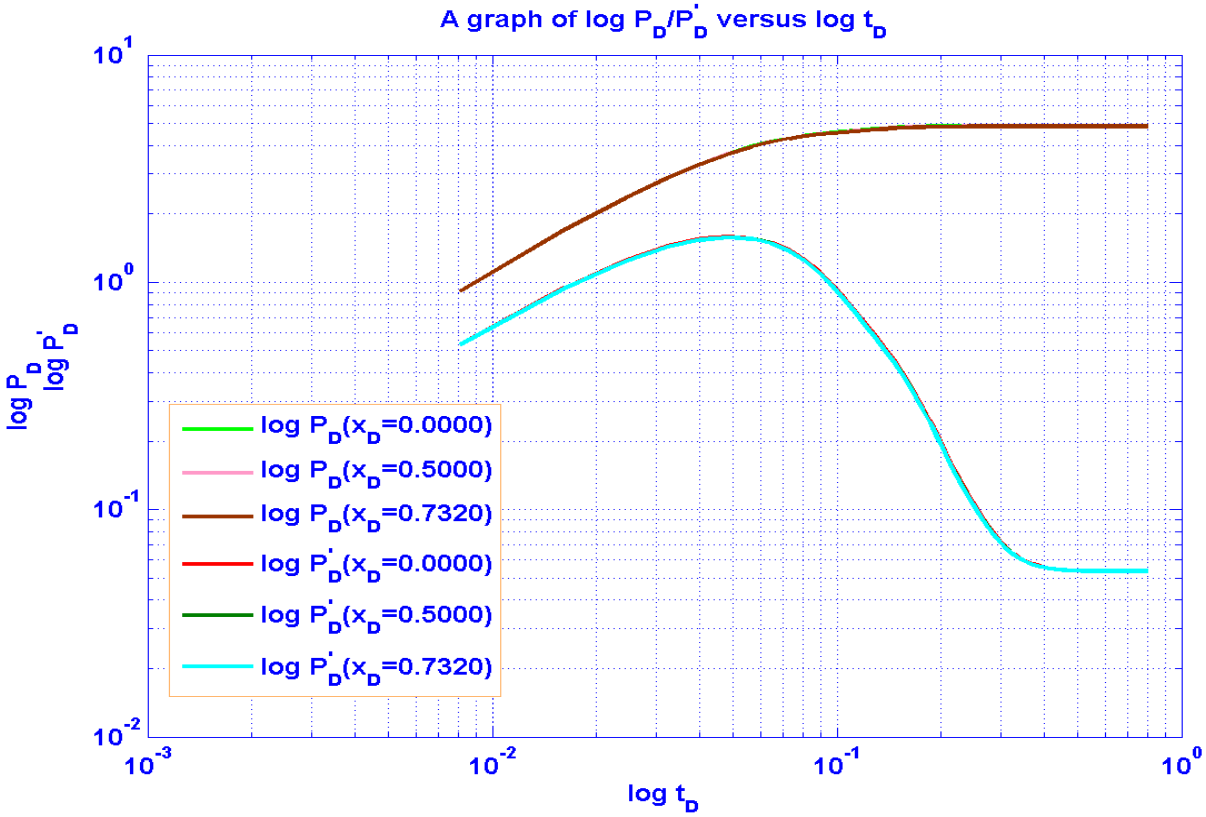

Figure 5: Graph of $\log P_D$ and $\log P'_D$ for all flow regimes, $L_D = 4.6675$

Table VI: P_D and P'_D with varying t_D for all flow regimes, $L_D = 5.8344$

	$L_D = 5.8344$, $y_{eD} = 0.3503$, $h_D = 0.1566$					
	x_D	0.0000	0.5000		0.7320	
	$\propto$	8.4772	8.6521		8.6415	
	$\propto_1$	20.917	20.917		20.917	
t_D	P_D	P'_D	P_D	P'_D	P_D	P'_D
0.00	0.0000	0.0000	0.0000	0.0000	0.0000	0.0000
0.05	4.6157	2.3313	4.5968	2.3056	4.5980	2.3071
0.10	5.9673	1.6224	5.9260	1.5867	5.9285	1.5888
0.15	6.4274	0.8687	6.3728	0.8408	6.3760	0.8424
0.20	6.5817	0.4279	6.5205	0.4107	6.5242	0.4117
0.25	6.6312	0.2115	6.5671	0.2021	6.5709	0.2026
0.30	6.6451	0.1137	6.5798	0.1090	6.5837	0.1093
0.35	6.6475	0.0719	6.5817	0.0696	6.5856	0.0698
0.40	6.6465	0.0544	6.5805	0.0534	6.5844	0.0535
0.45	6.6448	0.0474	6.5787	0.0469	6.5826	0.0470
0.50	6.6432	0.0446	6.5770	0.0444	6.5810	0.0444
0.55	6.6419	0.0435	6.5757	0.0434	6.5796	0.0434
0.60	6.6407	0.0431	6.5745	0.0430	6.5784	0.0430
0.65	6.6399	0.0429	6.5737	0.0429	6.5776	0.0429
0.70	6.6392	0.0428	6.5730	0.0428	6.5769	0.0428
0.75	6.6387	0.0428	6.5725	0.0428	6.5764	0.0428
0.80	6.6383	0.0428	6.5721	0.0428	6.5760	0.0428

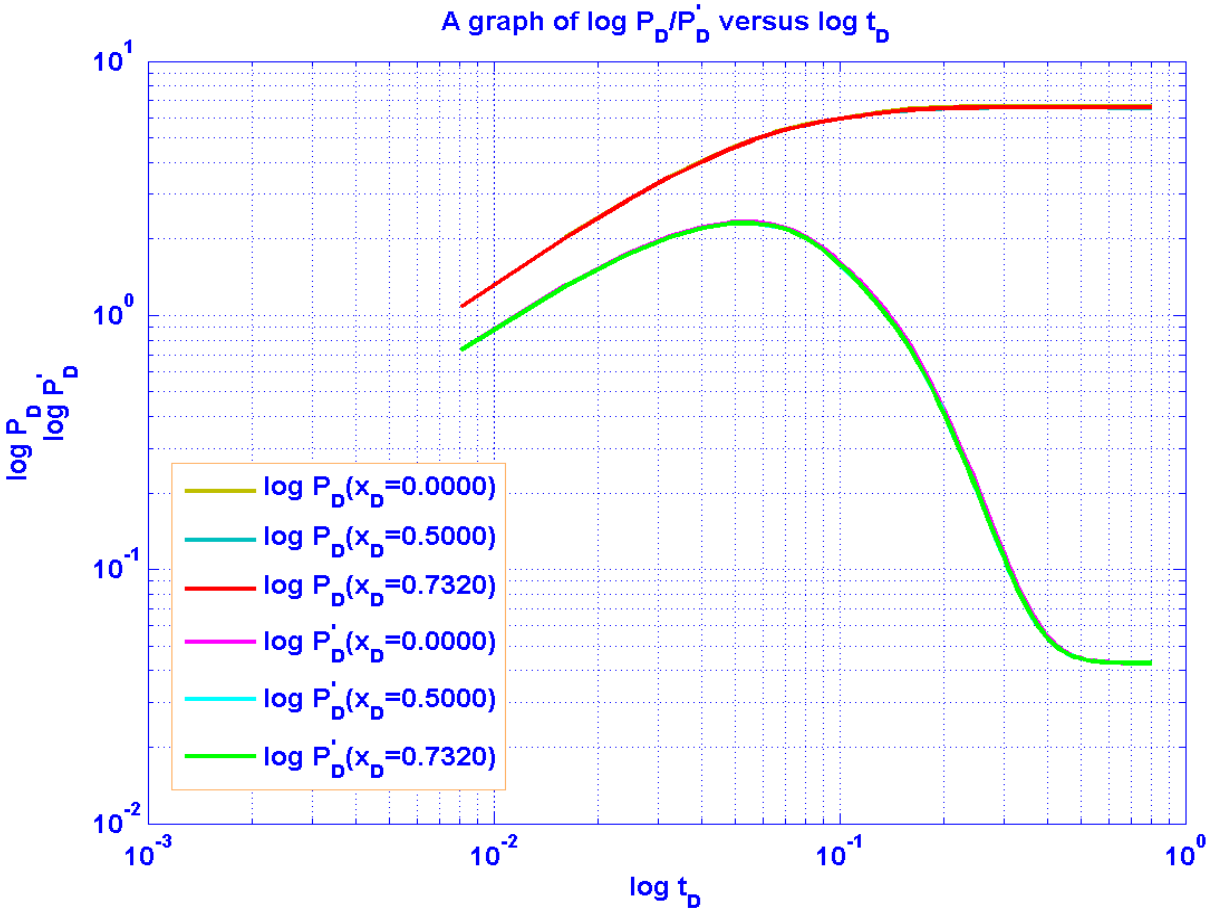

Figure 6: Graph of $\log P_D$ and $\log P'_D$ for all flow regimes, $L_D = 5.8344$

Table VII: P_D and P'_D with varying t_D for all flow regimes, $L_D = 7.0013$

	$L_D = 7.0013, y_{eD} = 0.2919, h_D = 0.1305$					
	x_D	0.0000	0.5000		0.7320	
	$\propto$	4.3863	4.6448		4.5741	
	$\propto_1$	10.823	10.823		10.823	
t_D	P_D	P'_D	P_D	P'_D	P_D	P'_D
0.00	0.0000	0.0000	0.0000	0.0000	0.0000	0.0000
0.05	6.4552	4.5388	6.4096	4.4636	6.4219	4.4839
0.10	9.8157	5.1993	9.6864	5.0272	9.7213	5.0732
0.15	11.748	4.5138	11.538	4.2918	11.594	4.3504
0.20	12.861	3.4971	12.585	3.2710	12.659	3.3300
0.25	13.501	2.5472	13.177	2.3447	13.263	2.3969
0.30	13.868	1.7864	13.510	1.6194	13.605	1.6619
0.35	14.077	1.2227	13.697	1.0923	13.797	1.1251
0.40	14.195	0.8243	13.799	0.7267	13.904	0.7510
0.45	14.261	0.5515	13.855	0.4807	13.962	0.4981
0.50	14.296	0.3691	13.884	0.3189	13.993	0.3311
0.55	14.315	0.2489	13.899	0.2142	14.008	0.2225
0.60	14.324	0.1710	13.905	0.1473	14.015	0.1529
0.65	14.327	0.1211	13.906	0.1051	14.017	0.1088
0.70	14.327	0.0892	13.906	0.0786	14.016	0.0810
0.75	14.326	0.0690	13.904	0.0620	14.015	0.0636
0.80	14.324	0.0563	13.902	0.0518	14.013	0.0528

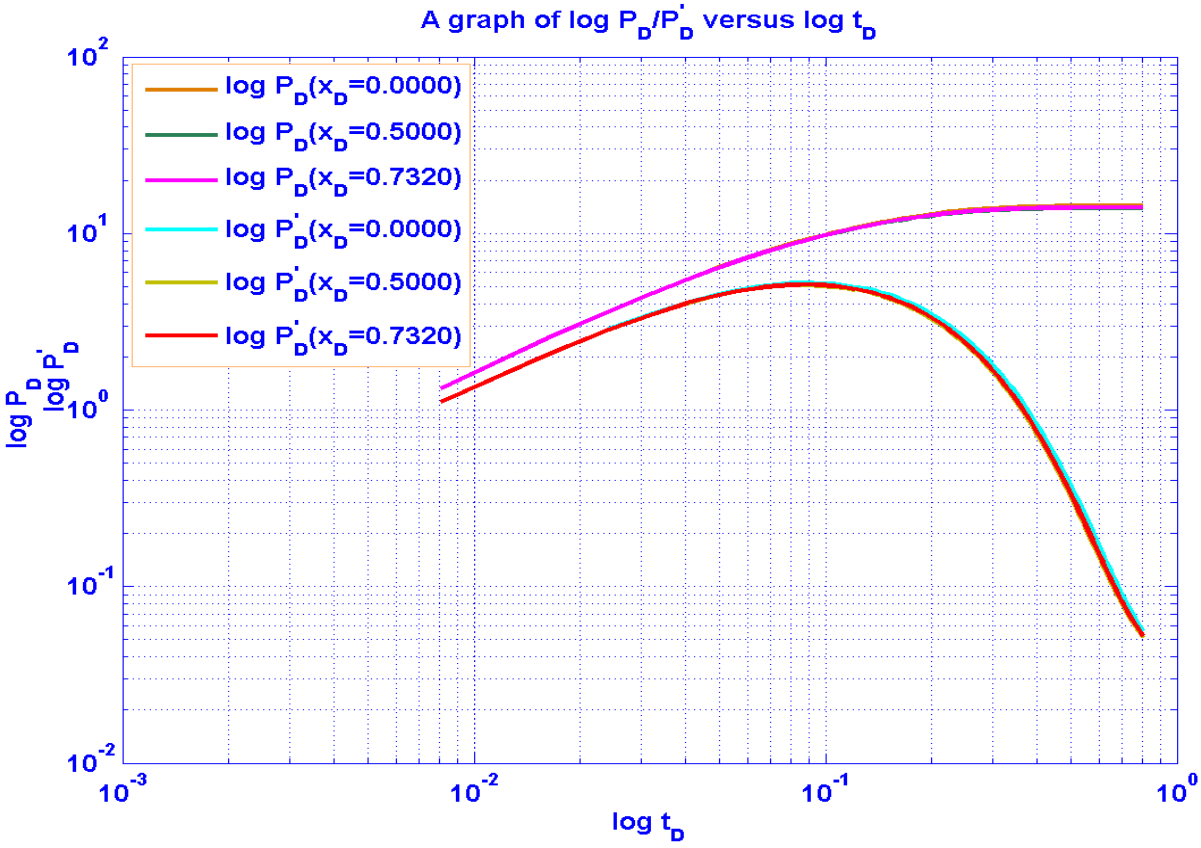

Figure 7: Graph of $\log P_D$ and $\log P'_D$ for all flow regimes, $L_D = 7.0013$

Table VIII: P_D and P'_D with varying t_D for all flow regimes, $L_D = 8.1681$

	$L_D = 8.1681, y_{eD} = 0.2502, h_D = 0.1119$					
	x_D	0.0000	0.5000		0.7320	
	$\propto$	0.5188	0.8547		0.6852	
	$\propto_1$	1.2801	1.2801		1.2801	
t_D	P_D	P'_D	P_D	P'_D	P_D	P'_D
0.00	0.0000	0.0000	0.0000	0.0000	0.0000	0.0000
0.05	9.1083	8.4346	9.0144	8.2520	9.0614	8.3432
0.10	17.052	15.592	16.697	14.921	16.874	15.253
0.15	24.461	21.799	23.705	20.411	24.079	21.090
0.20	31.390	27.159	30.116	24.891	30.742	25.989
0.25	37.877	31.763	35.993	28.504	36.912	30.065
0.30	43.955	35.686	41.384	31.372	42.630	33.415
0.35	49.647	38.996	46.330	33.596	47.928	36.125
0.40	54.983	41.755	50.873	35.267	52.841	38.272
0.45	59.984	44.020	55.049	36.467	57.396	39.927
0.50	64.672	45.842	58.887	37.262	61.621	41.148
0.55	69.067	47.267	62.418	37.715	65.541	41.993
0.60	73.185	48.338	65.666	37.877	69.177	42.508
0.65	77.048	49.093	68.657	37.792	72.552	42.738
0.70	80.669	49.569	71.413	37.505	75.684	42.723
0.75	84.064	49.795	73.951	37.045	78.591	42.495
0.80	87.248	49.804	76.292	36.446	81.290	42.088

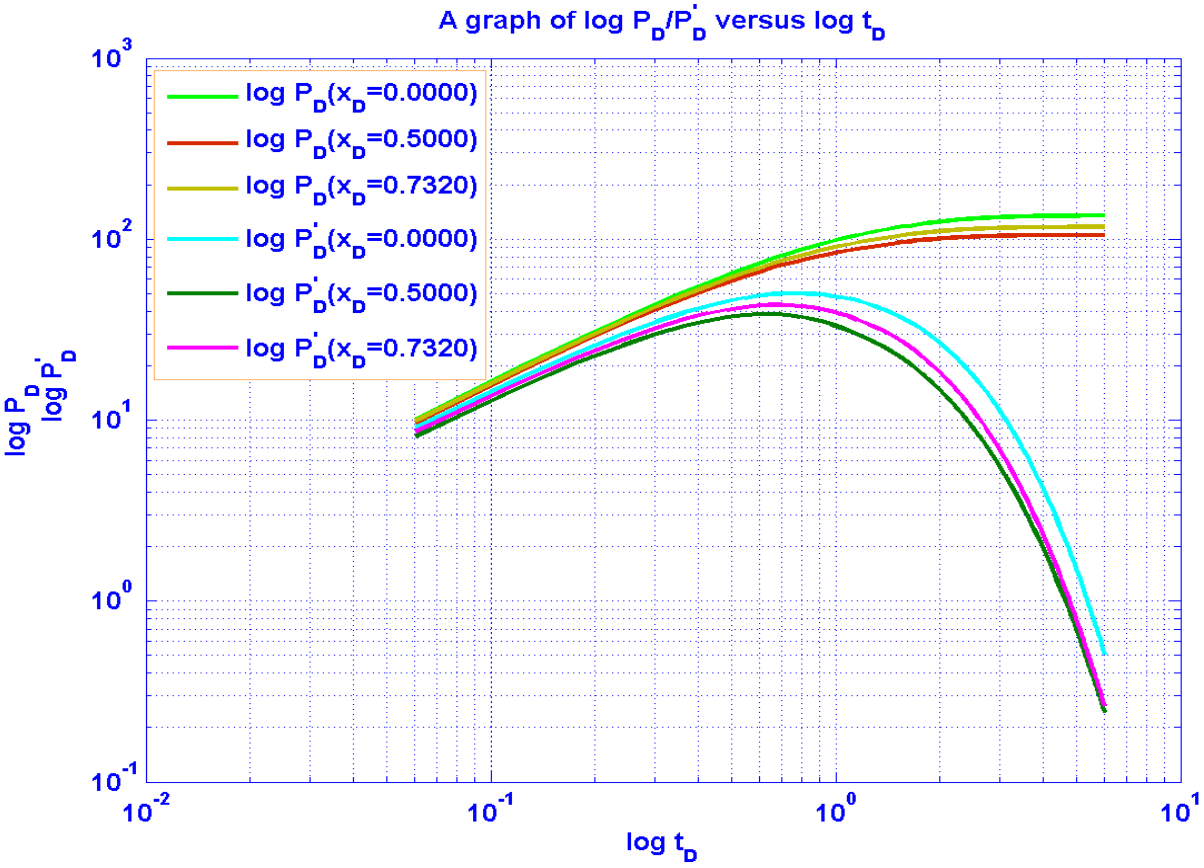

Figure 8: Graph of $\log P_D$ and $\log P'_D$ for all flow regimes, $L_D = 8.1681$

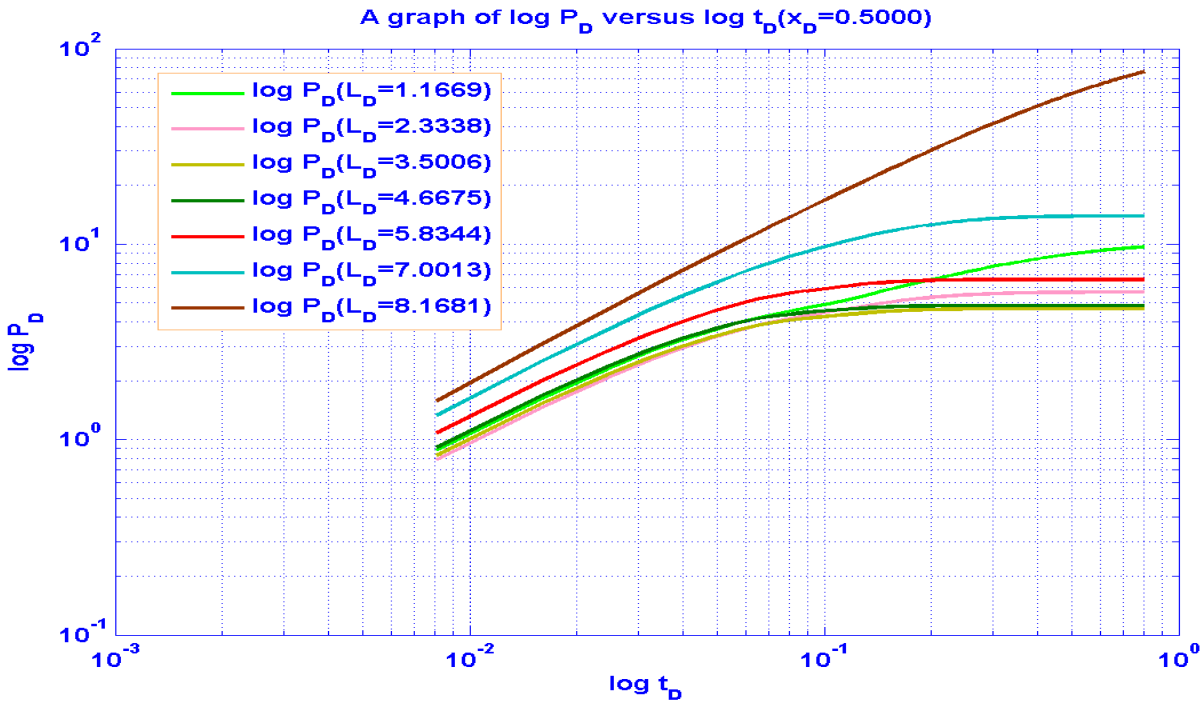

Figure 9: Graph of all $\log P_D$ for varying L_D for all flow regimes, $x_D = 0.5000$

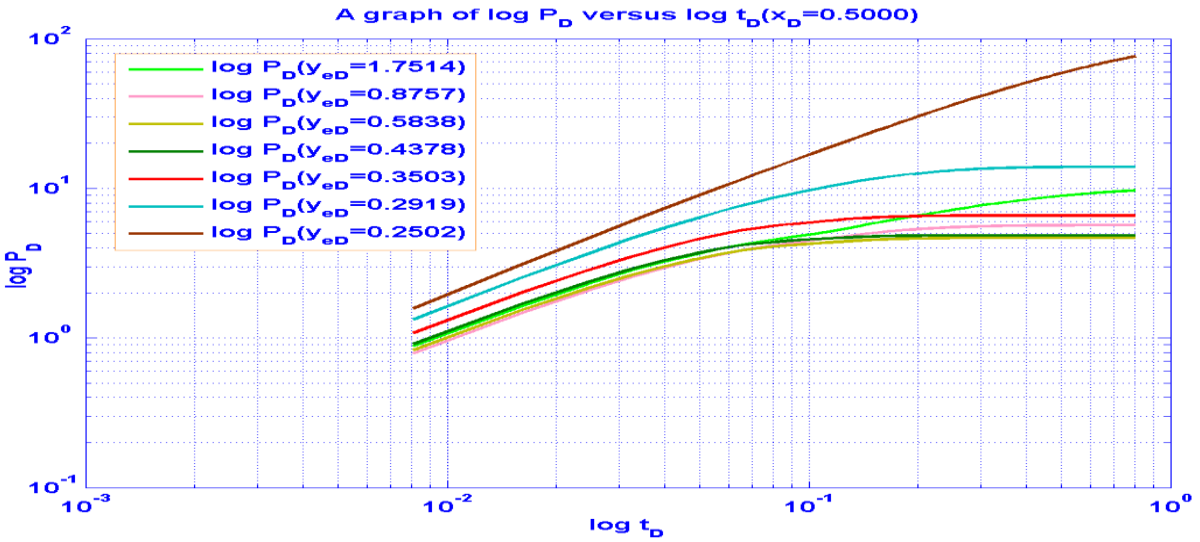

Figure 10: Graph of all log P_D for varying y_{eD} for all flow regimes, $x_D = 0.5000$

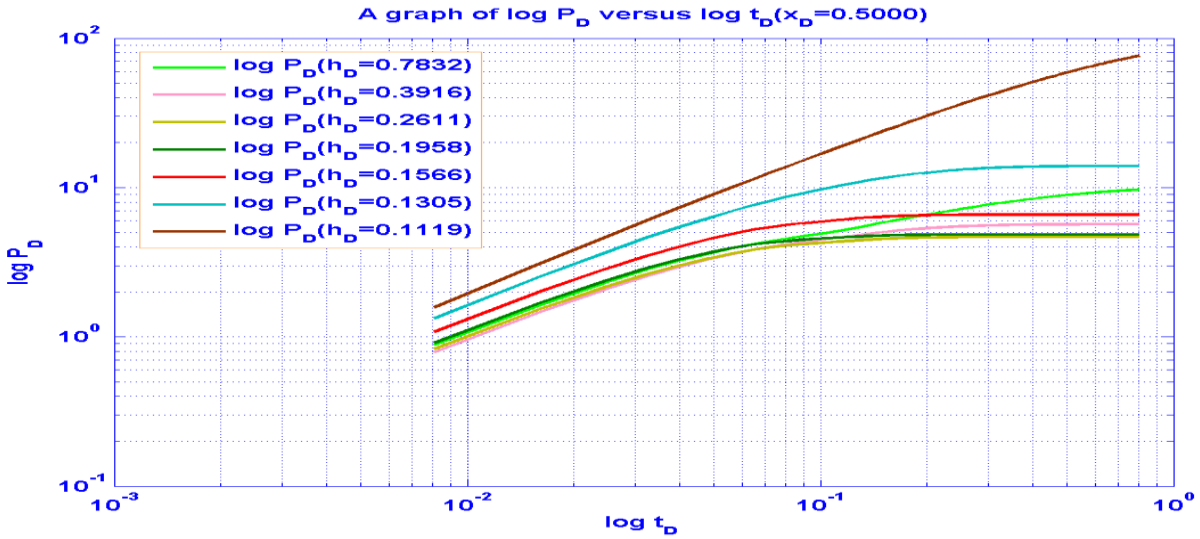

Figure 11: Graph of all log P_D for varying h_D for all flow regimes, $x_D = 0.5000$

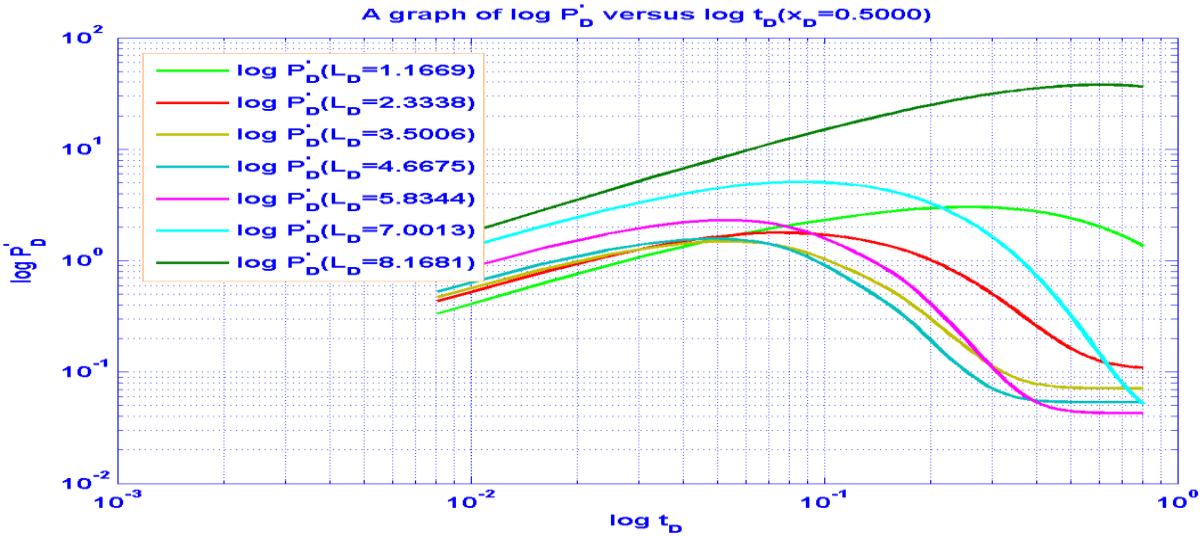

Figure 12: Graph of all log P'_D for varying L_D for all flow regimes, $x_D = 0.5000$

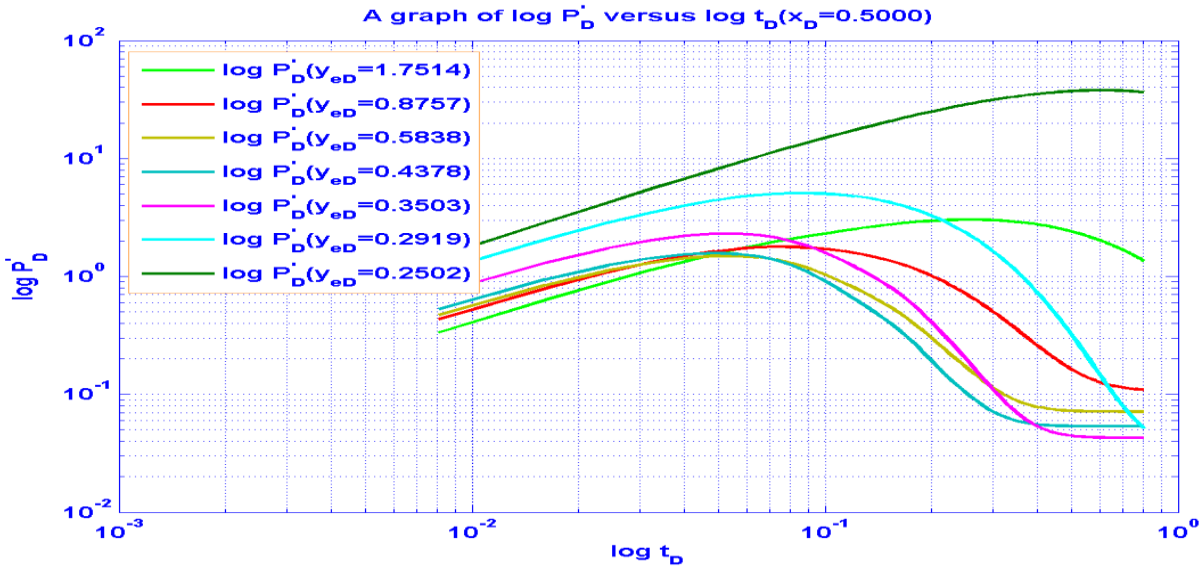

Figure 13: Graph of all log P'_D for varying y_{eD} for all flow regimes, $x_D = 0.5000$

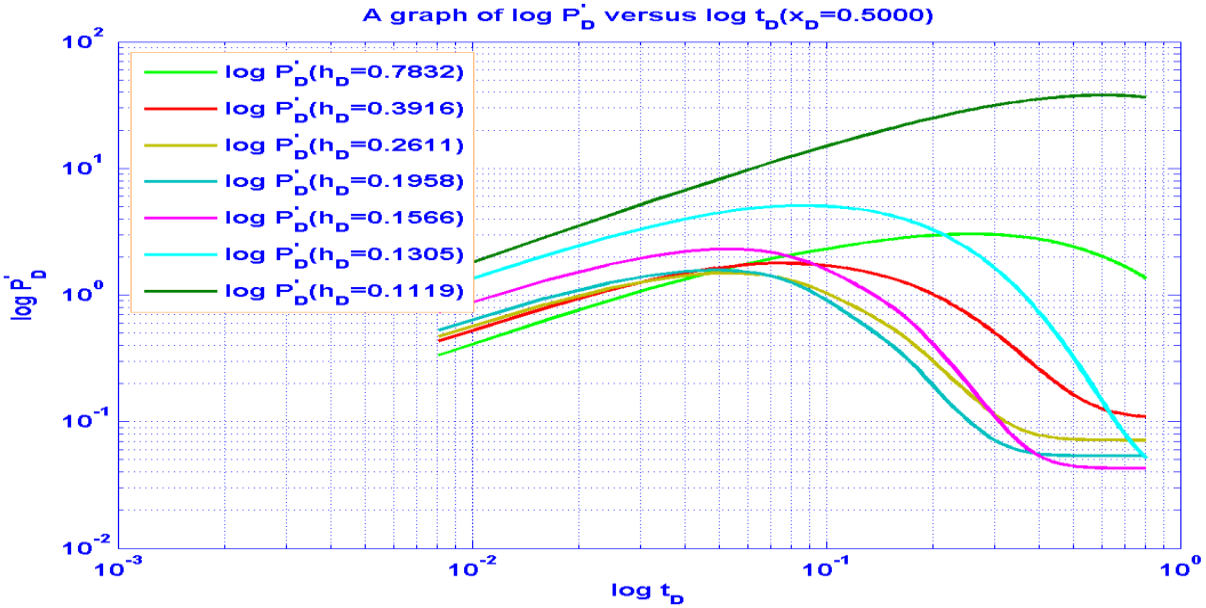

Figure 14: Graph of all log P'_D for varying h_D for all flow regimes, $x_D = 0.5000$

V. Results And Discussions

Table I shows the computed dimensionless variables for $x_D = 0.5000$. The results indicate that, the variation of x_D does not affect other dimensionless variables of a horizontal well in a rectangular reservoir geometry. From the calculations it clearly shows that, $r_{wD} = z_D - z_{wD}$, $y_{eD} = 2y_D$ and $y_D = y_{wD}$. Results from the table show that, $h_D, y_D, z_D, y_{wD}, z_{wD}, x_{eD}, y_{eD}, z_{eD}$ and r_{wD} vary inversely with L_D.

Table II to table VIII shows the computed values of P_D and P'_D with varying t_D for various values of L_D for all flow regimes. Results indicate P_D and P'_D vary directly with t_D until the breakthrough time when the P_D starts exhibiting a constant trend. At this breakthrough time P'_D shows a downward trend until it collapses to zero indicating that, the reservoir fluid has encountered a boundary. At this point the behavior of P'_D characterizes the unsteady, pseudo steady and steady state flow regimes.

Figure 1. describes an oil reservoir with a horizontal well specially designed away from water drives mechanisms to prevent early encroachment of the unwanted reservoir fluids. Figure 2 to figure 8 demonstrates a log-log plot of dimensionless pressure and dimensionless pressure derivative as the dimensionless well length is varied from $L_D = 1.1669$ to $L_D = 8.1681$. Results show that both dimensionless pressure and dimensionless pressure derivative varies directly with dimensionless time until at fluid breakthrough time when dimensionless pressure derivative potentially collapse gradually to zero when dimensionless pressure exhibits a constant trend

that is when the pressure does not change with time, $\frac{\partial P_D}{\partial t_D} = 0$. The effect of variation of x_D in dimensionless pressure and dimensionless pressure derivative is negligible.

Figure 9 show that dimensionless pressure varies directly with dimensionless well length until at fluid breakthrough time when dimensionless pressure exhibits a constant trend that is when the pressure does not change with time. Figure 10 show that dimensionless pressure varies inversely with dimensionless external reservoir width until at fluid breakthrough time when dimensionless pressure exhibits a constant trend that is when the pressure does not change with time. Figure 11 show that dimensionless pressure varies inversely with dimensionless pay thickness until at fluid breakthrough time when dimensionless pressure exhibits a constant trend that is when the pressure does not change with time. Figure 12 show that dimensionless pressure derivative varies directly with dimensionless well length until at fluid breakthrough time when dimensionless pressure derivative potentially collapses gradually to zero. Figure 13 show that dimensionless pressure derivative varies inversely with dimensionless external reservoir width until at fluid breakthrough time when dimensionless pressure derivative potentially collapses gradually to zero. Figure 14 show that dimensionless pressure derivative varies inversely with dimensionless pay thickness until at fluid breakthrough time when dimensionless pressure derivative potentially collapses gradually to zero.

VI. Conclusions

Equation (38) is the P_D distribution in a reservoir having an edge constant pressure boundary at the upper end and a constant pressure boundary at the bottom. Equation (39) is the corresponding dimensionless pressure derivative of the reservoir for all flow regimes. The edge constant pressure is similar to edge water drive and the bottom constant pressure boundary is similar to bottom water drive frequently encountered in reservoirs. Effects of fluid, wellbore and reservoir properties on P_D and P_D' have been studied. The following conclusions can be deduced from the study where the models show clearly that: -

a. Fluid flow equation of pressure distribution for the early radial, early linear, late pseudo-radial and late linear flow regimes are defined by equations (17), (19), (24), (25), (30), (31), (36) and (37) respectively. From the equations: -
   i. The P_D and P_D' are particularly inversely affected by reservoir width, pay thickness and reservoir width.
   ii. Both dimensionless pressure and its derivatives are affected by reservoir dimensionless length, thickness, fluid properties and well design.
   iii. The models are capable of predicting actual constant pressure influences at all flow time.
b. From the final flow equations (39), the dimensionless pressure derivative graphs shows that the flow is characterized by: -
   i. Unsteady state flow regime also referred as transient state which is the fluid flowing condition at which the rate of change of pressure with respect to time at any position, i in the reservoir is not zero or constant that is $\left(\frac{\partial P}{\partial t}\right)_i = f(i,t)$
   ii. Pseudo steady state flow regime also referred as quasisteady state flow is when the pressure at different locations in the reservoir is declining linearly as a function of time that is $\left(\frac{\partial P}{\partial t}\right)_i = \text{constant}$
   iii. Steady state flows regime if the pressure at any location in the reservoir remains constant that is does not change with time, $\left(\frac{\partial P}{\partial t}\right)_i = 0$. The equation shows that the rate of change of pressure, P with respect to time, t at any location, i is zero.
c. For the well test procedure, the graphs clearly show the following: -
   i. The P_D will exhibit a constant trend with t_D at fluid breakthrough time.
   ii. The P_D' will, as a result of a constant P_D, potentially collapse gradually to zero at the moment the P_D begins to exhibit a constant trend at fluid breakthrough time.
   iii. Increase in dimensionless well length prolongs the fluid breakthrough for all well completions.
d. To determine the optimum longitudinal well length: -
   i. The position of the well adversely affects the clean oil production.
   ii. Maximum oil production is achieved on a higher dimensionless well length.
e. Identifying reservoir fluids, rock and wellbore properties, calculations clearly shows that, $r_{wD} = z_D - z_{wD}$, $y_{eD} = 2y_D$ and $y_D = y_{wD}$ and from the tables, results show that, $h_D, y_D, z_D, y_{wD}, z_{wD}, x_{eD}, y_{eD}, z_{eD}$ and r_{wD} vary inversely with L_D.

Competing interests

Authors have declared that no competing interests exist.

Dimensionless parameters

$$P_D = \frac{kh\Delta p}{141.2q\mu B} \qquad i_{wD} = \frac{2i_w}{L}\sqrt{\frac{k}{k_i}} \qquad L_D = \frac{L}{2h}\sqrt{\frac{k}{k_x}}$$

$$t_D = \frac{4kt_i}{\phi\mu c_t L^2} \qquad i_{eD} = \frac{2i_e}{L}\sqrt{\frac{k}{k_i}} \qquad h_D = \frac{1}{L_D}\sqrt{\frac{k^2}{k_x k_z}}$$

$$\eta_i = \frac{k_i}{\phi\mu c_t} \qquad h_D = \frac{2h}{L}\sqrt{\frac{k}{k_z}} \qquad i = x, y, z$$

$$i_D = \frac{2i}{L}\sqrt{\frac{k}{k_i}}$$

Acknowledgements

This work was supported by the National Research Fund-Kenya (NRF) grant funded by the Government of Kenya.

References

[1]. Gringarten, A. C. And Ramey, H. J. (October, 1973). The Use of Source and Green's Function in Solving Unsteady-Flow Problem in Reservoir. SPEJ. SPE 102118/3818-PA. 13(05). 285-295. Https://Doi: 10.2118/3818-PA

[2]. Daviau, F., Mouronval, G., Bourdarot, G. And Curutchet, P. (December, 1988). Pressure Analysis for Horizontal Wells, SPE Formation Evaluation, SPE, 3(4), 716-724. Https://Doi.Org/10.2118/14251-PA

[3]. Ozkan Erdal And Raghavan Rajagopal. (August, 1990). Performance Of Horizontal Wells Subject to Bottom Water Drive. SPE-18559-PA. 5(03). Https://Doi:10.2118/18559-PA

[4]. Freddy – Humberto Escobar, Javier – Andres Martinez and Matilde Montealegre-Madero. (2013). Pressure Transient Analysis for A Reservoir with A Finite – Conductivity Fault. Latino American Journal of Oil and Gas and Alternative Energy. 5 (2), 5-18

[5]. Ogbue, M.C. And E.S. Adewole, E.S. (September, 2013). Theoretical Investigation of Factors Affecting Water Breakthrough Time in a Horizontal Well Subject to Bottom Water Drive. Advanced Materials Research Trans Tech Publications, Switzerland. 824 (2013), 394-400 Https://Doi: 10.4028/AMR.824.394

[6]. Edobhiye, O. And Adewole, E.S. (5-7 August, 2014). Effects of Both Wellbore and Reservoir Properties on Dimensionless Pressure and Dimensionless Pressure Derivative Distribution of a Horizontal Well in A Reservoir Subject to Bottom Water, Gas Cap and Single Edge Water Drive Mechanisms. SPE Nigeria Annual International Conference and Exhibition, Lagos Nigeria. Https://Doi.Org/10.2118/172384-MS

[7]. Al Rbeawi, S. And Tiab, D. (2013). Transient Pressure Analysis of Horizontal Wells in a Multi Boundary System. American Journal of Engineering Research (AJER). SPE, University of Oklahoma. 2(4), 44-66

[8]. Eiroboyi, I. And Wilkie, S.I. (April,2017). Comparative Evaluation of Pressure Distribution Between Horizontal and Vertical Wells in A Reservoir with Edge Water Drive. Nigerian Journal of Technology (NIJOTECH) 36(2), 457– 460

[9]. Chukwuma, M.C. And Adewole, E.S. (January, 2017). Application Of Odeh and Babu Strategies for Determination of Flow Periods in A Horizontal Well in A Bounded Reservoir. Journal of the Nigerian Association of Mathematical Physics. 39, 245 - 248

[10]. Orene, J.J. And Adewole, E.S. (January 2020). Pressure Distribution of a Horizontal Well in A Bounded Reservoir with Constant Pressure Top and Bottom. Nigerian Journal of Technology (NIJOTECH). 39(1), 154 – 160

[11]. John Obarhire Oloro. (January, 2021). Model To Study Pressure Behavior of Horizontal Well Subjected by Both Bottom Water and Gas Cap at Late Time. Advances In Dynamical Systems and Applications. ISSN 0973-5321, © Research India Publications. Https://Www.Ripublication.Com/Adsa.Htm. 16 (01), 59-66

[12]. Matthews, C. S. And Russell, D.G. (1967). Pressure Buildup and Flow Tests in Wells. Monograph Series, 1. Society of Petroleum Engineers Of AIME, Dallas

[13]. Jiazheng Qin., Shiqing Cheng, Youwei He, Dingyi Li, Le Luo, Xinzhe Shen and Haiyang Yu., (November, 2018), Diagnosis of Water Influx Locations of Horizontal Well Subject to Bottom Water Drive Through Well Testing Analysis. Hindawi Geofluids. 2018, 1-14. Https://Doi.Org/10.1155/2018/6385252

[14]. Mutili Peter Mutisya, *et* al. (October, 2020), Effects of Fluid and Reservoir Characteristics on Dimensionless Pressure and Derivative of a Horizontal Well in a Bounded Oil Reservoir with Simultaneous Single Edge and Bottom Water Drive. IOSR Journal of Mathematics (IOSR-JM), 16(5), 1-13